

Enhancement of Structural, Electrochemical, and Thermal Properties of Ni-Rich $\text{LiNi}_{0.85}\text{Co}_{0.1}\text{Mn}_{0.05}\text{O}_2$ Cathode Materials for Li-Ion Batteries by Al and Ti Doping

Yehonatan Levartovsky,^{*[a]} Xiaohan Wu,^[b] Christoph Erk,^[b] Sandipan Maiti,^[a] Judith Grinblat,^[a] Michael Taliander,^[a] and Doron Aurbach^{*[a]}

Ni-rich layered oxides $\text{LiNi}_{1-x-y}\text{Co}_x\text{Mn}_y\text{O}_2$ ($1-x-y>0.5$) are promising cathode materials for the new generation of Li-ion batteries suitable for electro-mobility due to their high energy density, good rate capability, and relatively low cost. However, their main drawback is poor cycling performance, particularly at elevated temperatures. In this research, it is demonstrated how doping with Al and Ti, using straightforward solid-state mixing synthesis, can dramatically enhance the structural, electrochemical, and thermal properties of $\text{LiNi}_{0.85}\text{Co}_{0.1}\text{Mn}_{0.05}\text{O}_2$ (NCM85). The capacity retention of Al-doped and Ti-doped cathodes after 100 cycles at 100% DOD at 1 C and 45 °C using standard electrolyte solutions could reach nearly 99% and 78%,

respectively, while the capacity retention of the undoped material was less than 74% in similar experiments. Doping with Al and Ti facilitates the Li intercalation processes and reduces voltage hysteresis. Structural study of the cycled cathodes shows that doping with Al, and to a smaller extent with Ti, reduces the formation of cracks in the particles of the cathode materials upon cycling, consequently reducing degradation. Thermal studies show that doping with Al or Ti improves the thermal stability of these cathode materials. Highly interesting is the correlation between the morphology and thermal stability, impedance properties and the electrochemical characteristics as a function of doping.

1. Introduction

Rechargeable Li-ion batteries are playing a pivotal role in the revolution of microelectronics and serve as the main power sources for portable electronic devices. Their higher gravimetric and volumetric energy compared to other rechargeable battery systems have made them a pervasive, integral, and indispensable part of our daily life in the 21st century.^[1,2] Recently there has been considerable research interest in cathode materials denoted as Ni-rich NCM with the general formula $\text{LiNi}_{1-x-y}\text{Co}_x\text{Mn}_y\text{O}_2$ ($1-x-y>0.5$) with $\alpha-\text{NaFeO}_2$ structure. They are considered as promising candidates to replace the commonly used LiCoO_2 cathodes that serve as the positive electrodes in most of the Li-ion batteries in the market.^[3] Among the Ni-rich NCM cathode materials, $\text{LiNi}_{0.85}\text{Co}_{0.1}\text{Mn}_{0.05}\text{O}_2$ (denoted as NCM85) has received special attention due to its high initial discharge capacity. However, like many Ni-rich materials, it suffers from capacity degradation over prolonged cycling and thermal instability that is caused by extra surface reactivity structure instability which characterize the lithiated

transition metal oxide cathodes when the content of the Ni component is high. It appears that the high concentration of Ni in these materials affects both surface reactions with the electrolyte solutions and stresses development upon cycling, which are detrimental for long term stability.^[4]

Previous studies have demonstrated that these deficiencies can be circumvented by two related strategies – coating and doping the cathodic materials. Coating with appropriate materials (like Al_2O_3 , SiO_2 , etc.) diminishes the parasitic reactions of the cathode surface with the electrolyte solution and suppresses dissolution of the transition metal ions (Ni, Co, Mn) by forming a protective layer around the particles surfaces.^[5,6]

Doping processes, usually with multivalent metals, stabilizes the crystal structure of NCM type cathode materials.

Several recent publications have explored the benefits of doping NCM cathode materials by foreign multivalent metal elements. Metal ions, such as Al^{3+} , Ti^{4+} , W^{6+} , B^{3+} , Mo^{6+} , Zr^{4+} have been used to dope NCM materials and stabilize them.^[8–18] It is important to note that Al was used also as a major component in Ni-rich cathode materials. The most important material is $\text{LiNi}_{0.8}\text{Co}_{0.15}\text{Al}_{0.05}\text{O}_2$, denoted as NCA, that was extensively explored.^[19,20]

The materials on which we report herein belong to the NCM family (thus including manganese as one of the key metallic elements) and contain higher concentration of Ni 85 mol%. In our work Al or Ti cations were dopants at very low concentrations (0.3 mol%), what makes this work as new and novel. We emphasize also the relatively simple structure of the materials we studied in which the concentration of the elements was uniform throughout the particles.

[a] Y. Levartovsky, S. Maiti, J. Grinblat, M. Taliander, Prof. D. Aurbach
Department of Chemistry and BINA

BIU Institution from Nano-Technology and Advanced Materials
Bar-Ilan University
Ramat-Gan, 5290002, Israel
E-mail: Levarty@biu.ac.il
Doron.Aurbach@biu.ac.il

[b] X. Wu, C. Erk
BASF SE
Ludwigshafen 67056, Germany

 Supporting information for this article is available on the WWW under
<https://doi.org/10.1002/batt.202000191>

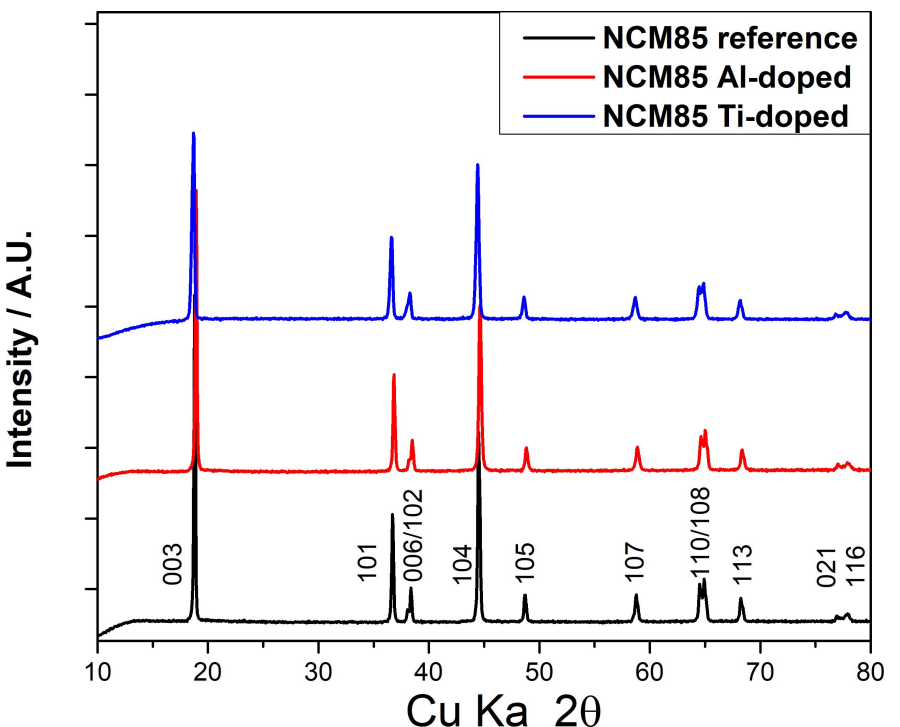


Figure 1. X-ray diffraction patterns of NCM85 reference and Al-doped and Ti-doped samples

Several studies have concluded that different dopants have distinct effects on the cathode materials, such as suppressing Li/Ni cation mixing, “pillar effect”, and impeding the intergranular cracks. The dopants’ effects on the cathode materials are influenced by several important properties, including ionic charge, ionic size, and magnetism.^[21] These effects help to explain the mechanisms through which these dopants at low concentration affect the behavior of NCM cathode materials (see later in the Results and Discussion Section).

It has been previously shown that doping NCM materials with lower Ni content than in NCM85 with Al or Ti, two relatively abundant light metals of high commercial importance, improves their electrochemical behavior and thermal characteristics.^[8–14]

However, such previous results may not indicate automatically that doping of NCM materials of higher content of Ni with these elements will be beneficial, because increase of the Ni content can change the structure, electrochemical response and capacity fading mechanisms.

Hence, each cathode material with a certain concentration of Ni has its own unique characteristics and response.

Here we show that doping NCM85 materials with only 0.3 mol% of Al enhances very coherently their electrochemical performances, safety features and structural stability. Doping with 0.3 mol% of Ti also demonstrated improvement in the performance of NCM85 cathodes, but to a lesser degree compared to doping with Al.

2. Results and Discussion

The XRD patterns of reference (undoped), Al-doped and Ti-doped NCM85 samples are shown in Figure 1. All the observed peaks are well indexed to a rhombohedral structure of the $\alpha - \text{NaFeO}_2$ type structure with a R-3 m space group, and without detectable impurity phases. This indicates that the doped samples retain the original single phase structure of the undoped, reference NCM85. The observable splitting of the (006)/(102) and (108)/(110) peaks indicated the existence of the layered structure with a hexagonal ordering in the samples. The intensity ratios of (003)/(104) of the NCM85 reference, Al- and Ti-doped are 1.60, 1.56, 1.16, respectively, also indicate a perfection of the layered structure with well-ordered distribution of Li and transition metals atoms in the corresponding layer for each composition.

The lattice constants and cell volumes of the samples are presented in Table 1. The values of the lattice constants a and c , and the cell volume V do not change dramatically upon doping, suggesting that the doping does not cause significant

Table 1. Lattice constants a and c and volume of uncycled and cycled samples

| Sample | a [Å] | c [Å] | V [Å ³] |
|------------------------|------------|------------|--------------------------|
| NCM85 reference | 2.870 | 14.188 | 101.22 |
| NCM85 Al-doped | 2.872 | 14.184 | 101.30 |
| NCM85 Ti-doped | 2.869 | 14.172 | 100.99 |
| Cycled NCM85 reference | 2.867 | 14.166 | 100.83 |
| Cycled NCM85 Al-doped | 2.858 | 14.187 | 100.36 |
| Cycled NCM85 Ti-doped | 2.865 | 14.175 | 100.74 |

structural changes in the crystal structure. The lack of structural changes in the lattice is reasonable since Al^{3+} and Ti^{4+} cations have similar sizes to Ni^{3+} cations. Hence, the crystallographic studies conducted so far could not explain the strong effect of doping on the electrochemical and morphological behavior described below.

Figure S1 shows high-resolution scanning electron microscope (HR-SEM) images of NCM85 reference (2a and 2b), Al-doped (2c and 2d) and Ti-doped (2e and 2f). As shown, all the samples share the same uniform morphology – spherical microstructure with secondary particles, with an average diameter of $10\ \mu\text{m}$, comprised of smaller primary particles. This finding is in agreement with previous morphological studies of Ni-rich NCM cathode materials.^[4,22] Thus, we conclude that doping with Al and Ti at the level used herein does not change the overall morphology.

Energy dispersive X-ray spectroscopy (EDX) was applied in conjunction with HR-SEM to investigate the elements content on the surface of the secondary particles of these materials. The spectra contain peaks of the expected metallic elements Ni, Co, Mn in an average ratio of 8.5:1:0.5 among them, reflecting roughly the true stoichiometry of the materials. The spectra of the doped samples show clearly Al and Ti peaks at atomic concentration higher by a factor of 5, compared to the overall bulk stoichiometry that was determined precisely in the synthesis. These results seem to reflect that there is some segregation in the distribution of the dopants, so their concentration on the surface is higher than that in the bulk, resulting from the final calcination process at elevated temperatures, which is the last stage of the synthesis. We analyzed such a phenomenon with Mo doped $\text{LiNi}_{0.8}\text{Co}_{0.1}\text{Mn}_{0.1}\text{O}_2$ samples using TOF-SIMS measurements, with which such segregation phenomena can be analyzed precisely.^[15] Further structural characterization of the different samples was carried out using transmission electron microscopy (TEM) analysis (Figure 2). With the NCM85 reference samples, the vast majority of grains analyzed by TEM were, as expected, identified as the rhombohedral phase described by the $R\bar{3}\ m$ space group. However, in a few cases we observed grains with integration of a major rhombohedral $\text{Li}(\text{TM})\text{O}_2$ component with the minor

Li_2MnO_3 monoclinic component. Figure 2a represents a general view of the microstructure consisting of grains 200–300 nm in size. The selected area electron diffraction (Figure 2b) taken from grain #1 contains, however, not only the pattern characteristic of the rhombohedral phase, but also an additional diffraction spots which were indexed in terms of the monoclinic phase. The dark field presented in Figure 2c, taken with the monoclinic reflection, shows an enlarged view of the grain #1, in which one can see bright fine plates of the monoclinic phase within a dark rhombohedral matrix.

The results of the TEM analysis of doped materials are similar to those of the reference material. The microstructure of all the samples consists of elongated grains, characterized by a layered rhombohedral structure. The microstructure of NCM85 Al- and NCM85 Ti-doped materials and examples of the selected area and the nano-beam diffractions, which indicate the presence of the rhombohedral phase $\text{Li}(\text{TM})\text{O}_2$, are shown, respectively, in Figure S2a–c and Figure S2a–c, respectively.

Results of electrochemical performance tests are presented in Figure 3. The data presented herein results from several parallel coherent experiments and the numbers provided are average values with a maximal deviation of $+/- 2\%$. The initial charge-discharge voltage profiles of the NCM85 reference, Al-doped and Ti-doped electrodes measured galvanostatically at 0.1 C rate in the potential range 3.0–4.3 V at 30 °C are shown in Figure 3a. The voltage profiles of the three types of electrodes are similar, apparently smooth and sloping, reflecting intercalation/de-intercalation processes that form mostly solid state solutions. However, a closer examination of their electrochemical response by derivatives of the voltage profiles (Figure 4) shows that Li intercalation/de-intercalation processes of these materials involve also phase transition stages. Ti-doped samples showed higher initial charge and discharge capacities (around $214\ \text{mAh g}^{-1}$) compared to that of the reference and Al-doped materials (around $209\ \text{mAh g}^{-1}$). We suggest that the slightly higher capacity of the Ti-doped material can result from expansion of the Li-ion channels in the active mass due to the doping, but we could not prove it yet. The first cycle coulombic efficiencies of these electrodes were around 90%, reflecting unavoidable initial irreversibility which is required for the

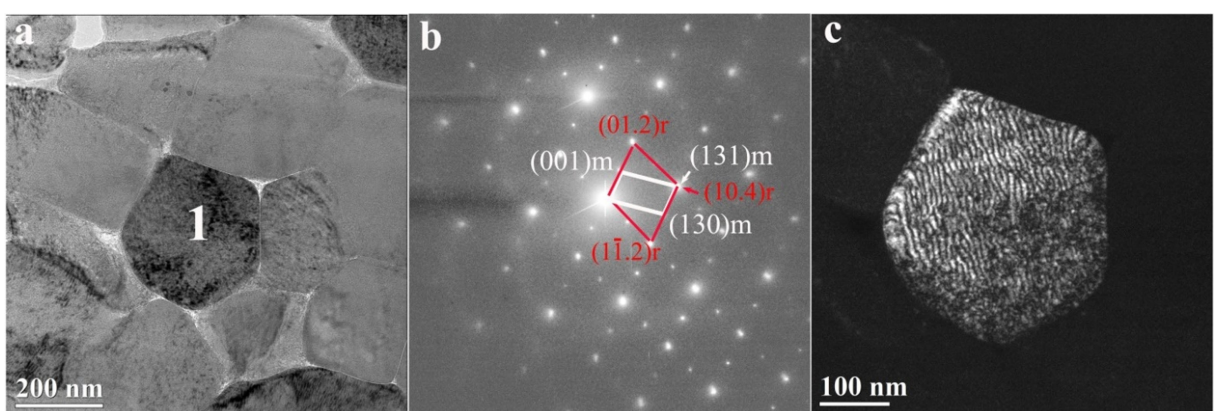


Figure 2. TEM analysis of NCM85 reference. a) TEM bright field image; b) SAD image taken from a 200 nm diameter area. Labels "r" and "m" denote rhombohedral and monoclinic phase, respectively. c) Dark field image taken from the grain # 1

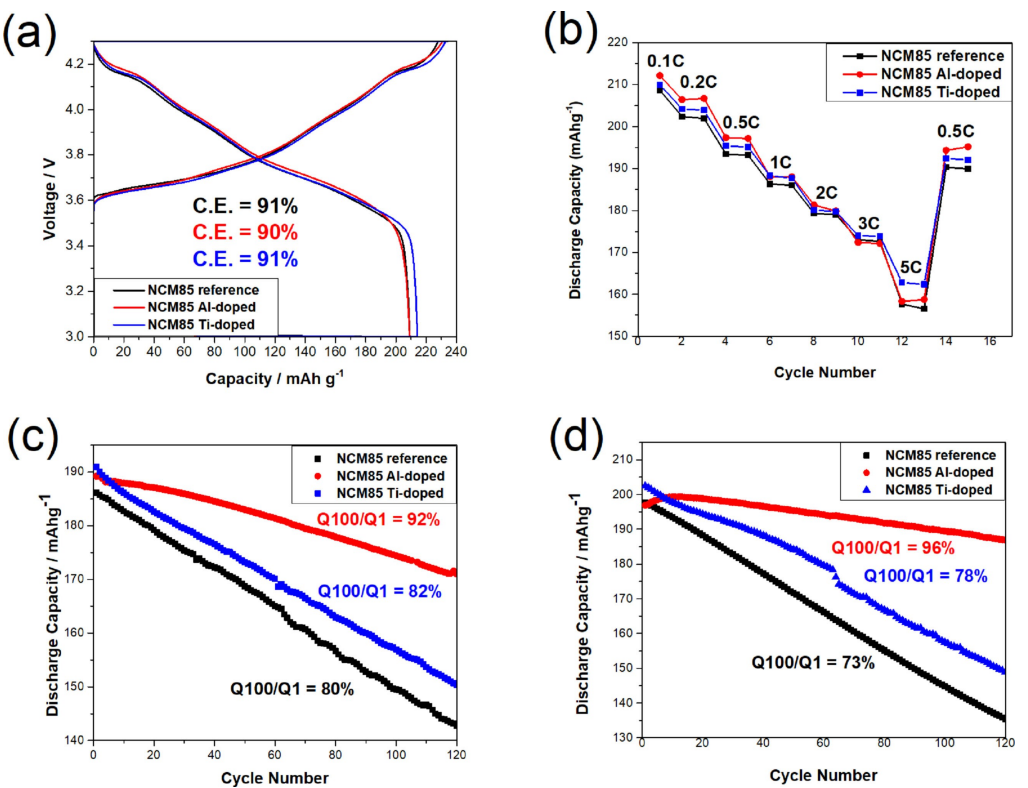


Figure 3. Electrochemical performance measurements of half-coin cells with Li metal anodes a) Initial charge and discharge curves of NCM85 reference, Al-doped and Ti-doped samples at a 0.1 C rate at 30 °C; b) Rate capability test of the samples at 30 °C; c) Cycling performance of the samples at 1 C at 30 °C; d) Cycling performance of the samples at 1 C at 45 °C. The solutions were 1 M LiPF₆ in EC-EMC 3:7 by volume.

rearrangement processes that bring these composite electrodes to their steady state during consequent cycling (in which 100% cycling efficiency can be reached).

Figure 3b shows rate capability tests of coin-cells comprising the different cathode materials vs. Li metal foil counter electrodes in solutions containing 1 M LiPF₆ and 3:7 mixtures of ethylene carbonate and ethyl-methyl carbonate (standard

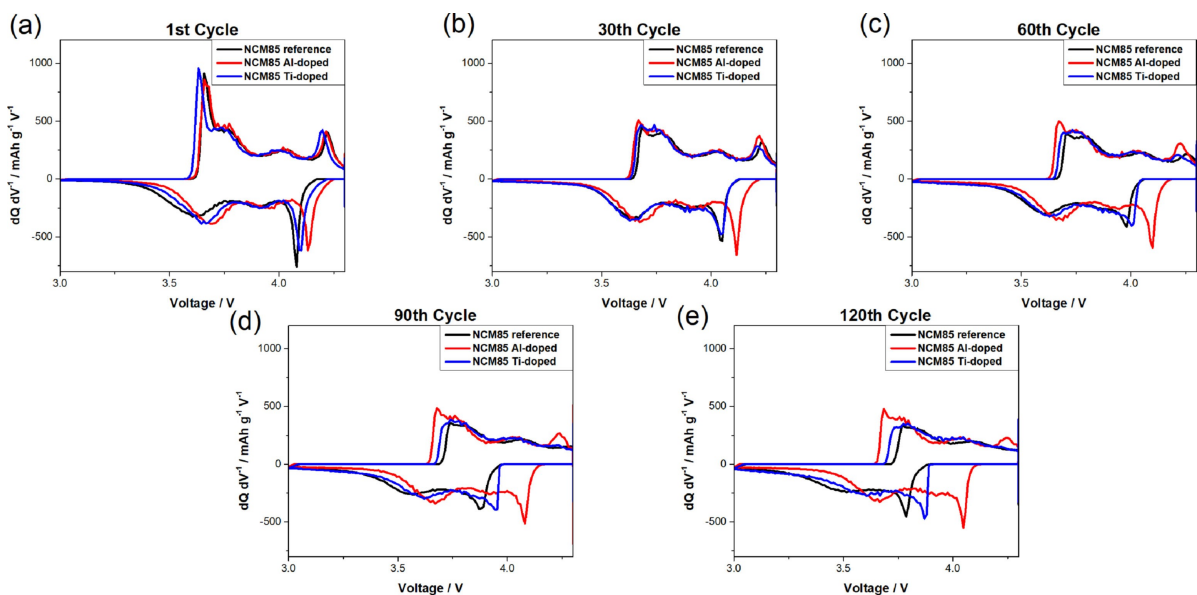


Figure 4. Differential capacity vs. voltage curves of 1st, 30th, 60th, 90th and 120th cycle for NCM85 reference, Al-doped and Ti-doped cathodes tested in half coin-cell using Li metal anodes at discharge rate of 1 C

solutions) at 30°C. The cells were charged at a rate of 0.5 C and discharged at 0.1, 0.2, 0.5, 1, 2, 3, and 5 C rates in the potential range of 3.0–4.3 V. Both Al-doped and Ti-doped NCM85 electrodes exhibit better rate capability than the reference electrodes, both at low and high rates. For example, the discharge capacity of NCM85 reference electrodes at 5 C was around 157 mAh g⁻¹, while the discharge capacity of the Al-doped and Ti-doped samples were around 159 mAh g⁻¹ and 163 mAh g⁻¹, respectively. These results indicate that doping with Al and Ti stabilizes the structure of this cathode material in a way that reduces the polarization which is responsible for the capacity drop-off at high rates.

The cycling performance of these electrodes at 30°C and 45°C is shown in Figure 3c and Figure 3d, respectively. After 5 formation cycles at 0.1 C, the cells were charged at 0.5 C and discharged at 1 C between 3.0 to 4.3 V for 120 cycles. In general, after several first cycles, the cycling efficiencies of the cells we measured approaches 100%. It is evident that the electrodes comprising the doped materials show higher capacity and stability compared to the reference electrodes in both temperatures. The initial specific discharge capacity of the electrodes containing the Al- and Ti-doped materials are higher by around 3 and 5 mAh g⁻¹ compared of that of the reference electrodes at 30°C. The electrodes comprising the Al-doped material exhibit impressive stability compared to the other electrodes explored in the present study: >92% capacity retention after 100 cycles, compared to around 82 and 80% relevant to electrodes with the Ti-doped and reference NCM85 materials (respectively) at 30°C; >96, around 78 and 73% for the electrodes containing Al, Ti-doped and reference NCM85 materials (respectively). In fact, Figures 3c and 3d show that the Ti-doped material is advantageous over the reference one mostly by a slightly higher specific capacity, while the capacity retention behavior of these two materials during electrodes cycling is rather nearly similar.

The electrochemical analysis includes a presentation of compared capacity/voltage derivatives (dQ/dE) vs. E curves of the 3 types of electrodes obtained from the voltage profiles of cells at the 1st, 30th, 60th, 90th, and 120th cycles during galvanostatic cycling experiments (Figure 4). The derivative curves of the first cycle for the three types of electrodes are very similar, showing three main sets of anodic and cathodic peaks centered around 3.6, 4.0 and 4.2 V vs. Li. These peaks can be attributed to multiphase transitions of hexagonal to monoclinic (H1→M), monoclinic to hexagonal (M→H2), and hexagonal to hexagonal (H2→H3) phases.^[4] It should be noted that for the Al-doped material, the picture is sharper: the potential difference between the anodic and cathodic peaks of the three couples is slightly smaller (clearly visible for the set of peaks around 4.2 V). The effect of cycling on this comparative potentiodynamic picture is interesting and significant: for the electrodes comprising the Al-doped NCM85, the electrochemical response as a function of cycle number, presented in the charts of Figure 4, become less sharp, but still resembles the response recorded in the first cycle even after 120 cycles. In turn, the electrochemical response of the NCM85 reference (undoped) electrodes, changes gradually upon cycling. There is

a pronounced shift of the major cathodic peak initially around 4.1 V, to lower potentials and the entire response become less pronounced, fuzzy and more featureless. Interestingly, the electrodes comprising Ti-doped NCM85 show an intermediate behavior, in terms of the shift to the lower voltage regime of the main cathodic peak and sharpness of the electrochemical response.

This behavior correlates well with data presented in Figures 3c and 3d, which demonstrates a relatively high stability of the Al-doped NCM85 electrodes and much lower stability of both Ti-doped and reference NCM85 electrodes.

Figure 5 shows the evolution of the average voltage hysteresis during galvanostatic cycling of the different electrodes at 30 °C using a charging rate of 0.5 C and discharge rate of 1 C. The hysteresis per cycle was calculated from the difference in the mean charge and discharge voltages presented in Figure S4. This electrochemical characterization of the electrodes is important to evaluate the specific energy of these systems, which is the product of the voltage and specific capacity. It is evident that both NCM85 Al- and Ti-doped materials exhibit lower voltage hysteresis compared to the reference material, with the former having remarkably low voltage hysteresis of 0.68 mV/cycle and much lower increase in average voltage per process during cycling, compared to the other electrodes (Figure S4).

Electrodes after 120 cycles underwent post-mortem analysis. Particles of the NCM85 active mass were cut by a focused-ion beam (FIB-SEM) system. SEM images of selected but very representative particles of these electrodes are presented in Figure 6. These images show indeed pronounced differences in the morphology of the cross sections of the three types of electrodes: The image related to the cycled reference electrodes shows very pronounced cracks all over the cross sections of the particles, while the cross sections of the cycled Al-doped NCM85 particles looks smooth, with no cracking. In turn, the images related to cycled Ti-doped NCM85 particles show an intermediate picture: the cross sections' image show some cracking, but to a much lesser extent compared to the case of the reference electrodes. These results are well in line with many previous studies on the stabilization of Ni-rich NCM cathode materials. It is widely accepted that a major capacity fading mechanism of these materials relates to strains and stresses resulting from repeated phase transitions during the exchange of Li ions (anisotropic volume changes), especially at the high potentials > 4 V.^[23,24] These stresses lead to the formation of cracks that propagate throughout the particles (as presented well in Figure 5). These cracks form very active surface area of the active mass that readily reacts with solution species which penetrate through the cracks inside the particles. These processes destroy the ordered structure of the cathode materials and degrade the cathodes because they electrically isolate increasing amounts of active mass during cycling. Doping with Al stabilizes the structure of these materials, while the effect of doping by Ti is much minor. Hence, the data presented in Figures 3, 4, 5 and 6 are very coherent, showing excellent correlation between structural and electrochemical stability. The lattice parameters and cell volumes of the samples

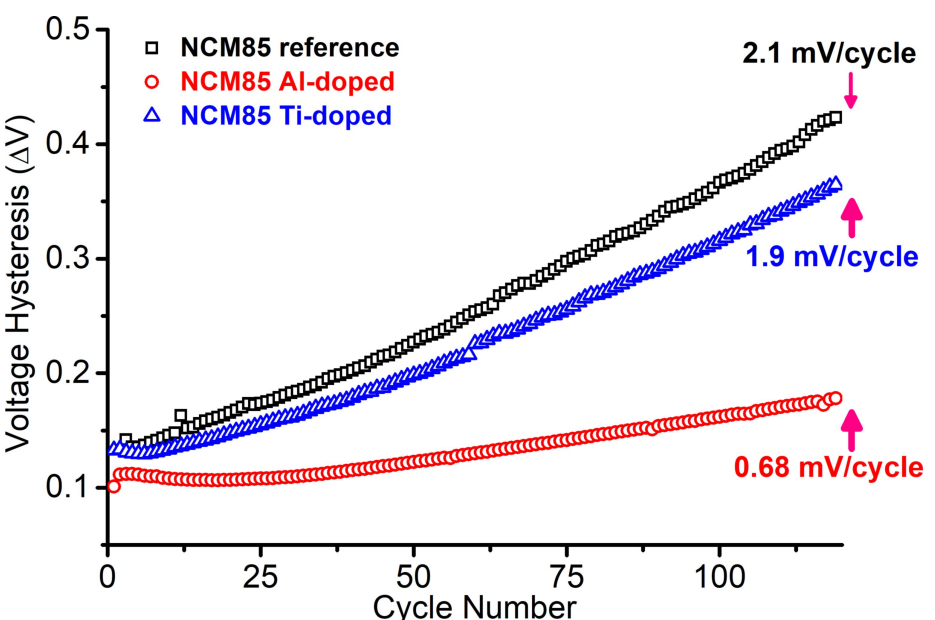


Figure 5. Voltage hysteresis ($\Delta V = V_{\text{charge}} - V_{\text{discharge}}$) of electrodes comprising NCM85 reference, Al-doped and Ti-doped materials at 30 °C.

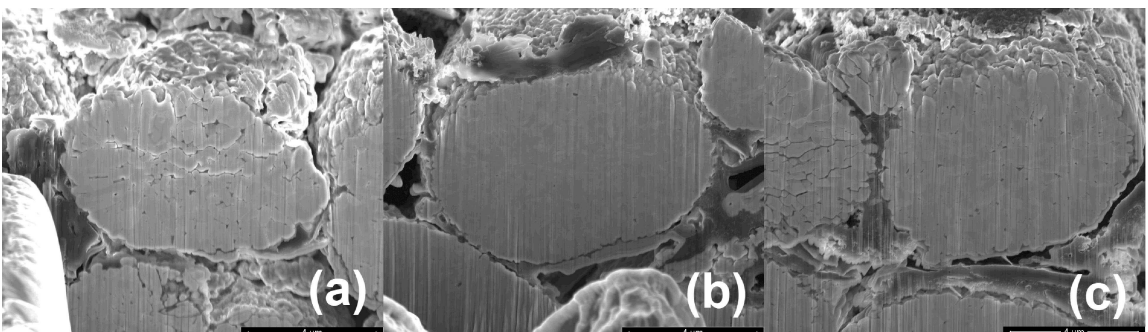


Figure 6. SEM images of FIB-cut electrodes: a) NCM85 reference, b) Al-doped, and c) Ti-doped after 120 cycles at 30 °C.

calculated from XRD of the cycled cathodes are presented in Table 1. The lattice parameters and the cell volumes do not change significantly after cycling, with the cell volumes slightly decrease. This finding strengthens the conclusion that the major degradation mechanism of these materials relates to the above described morphological changes, rather than to crystallographic aspects.

Electrochemical impedance spectroscopy (EIS) measurements were also carried out in order to evaluate the influence of doping on major time constants of these composite electrodes. It is important to note that EIS data of such composite electrodes have only qualitative importance, since it is impossible to unambiguously assign impedance spectral features to time constants of the electrochemical processes that the active mass undergoes. Nevertheless, the fact that all the electrodes were prepared nearly identically and they underwent the same electrochemical processes, enable a useful qualitative comparison among them, thus helping to further evaluate the effect of doping. Obvious features that affect the impedance of these NCM electrodes are: surface films formed by reactions of

the electrophilic and slightly acidic electrolyte solutions with the basic cathode materials through which Li ions have to migrate; interfacial charge transfer; the red-ox activity of the active mass in which the oxidation state of the transition metal cations changes as a function of the Li ions content; the solid state diffusion of Li ions in the bulk and finally, the capacitive behavior of the electrode, which content of Li ions depends on its temporary equilibrium potential (set by the experimental condition).^[19] Nyquist plots of Al-, Ti-doped and reference NCM85 cathodes vs. Li reference and counter electrodes, measured after 1st and 90th cycles at 30 °C at 4.0 V vs. Li in equilibrium during charging are presented in Figure 7. The spectra contain high and medium frequency arcs that can be roughly assigned to surface and bulk charge transfer processes (respectively) and a sloping line in the low frequencies that can be assigned to bulk diffusion processes.^[19] Interestingly, the spectra of the electrodes comprising the doped materials after a first cycle are nearly similar, while the spectrum of the reference electrodes exhibit higher impedance (spectacular in Figure 7a). The spectra of the electrodes after 90 cycles reflect

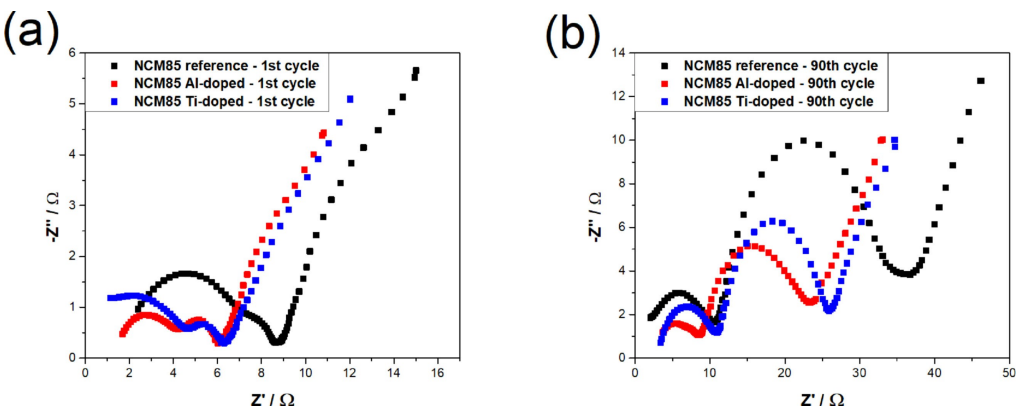


Figure 7. EIS plots of electrodes comprising Al-, Ti-doped and reference NCM85 materials (indicated) after 1 and 90 cycles (a,b) measured at 4 V (around equilibrium) in the course of charging. The electrolyte solution used was 1 M LiPF₆ in EC-EMC 3:7 by volume, 30 °C.

(as expected) a general increase in their impedance due to cycling. They also show clearly a much higher impedance of the reference electrodes and lowest impedance features of electrodes comprising the Al-doped NCM85. The spectra of the electrodes with the Ti-doped active mass are similar to the former ones, showing higher impedance features as clearly seen in Figure 7b. Interestingly, the reference electrodes which contain cracked particles and hence their active mass is supposed to develop high specific surface area, exhibit higher impedance, although high specific surface area should lead to lower interfacial and charge transfer resistances. It can be concluded that the cracks that are developed upon cycling do not add more active surface area for electrochemical interactions in equilibrium, because the parasitic reactions with solution species fill the cracks with the side reactions products. In turn, the cracking and particles disintegration should lead to detachment of active materials in the composite electrodes from the current collectors, thus explaining well the overall increase in the electrodes' impedance.^[25] Concluding this part, the EIS measurements are in excellent agreement with all the other observations described above, showing the clear positive influence of Al doping on the behavior of NCM85 cathodes (much lower impedance features) and a much lower positive effect by doping with Ti. Hence, there is a clear connection among structure stabilization, electrochemical cycling stability and lower impedance of these composite electrodes that are all caused by doping.

The enhanced cycling stability of the doped materials due to improved structural stability is even more evident in cycling tests of full cells (pouch cells containing NCM85 cathodes and graphite anodes) presented in Figure 8. After formation cycles, the full cells were charged at 0.5 C and discharged at 1 C between 3.0 to 4.3 V during 500 cycles. Cells comprising doped cathodes showed much higher stability compared to the cells containing the reference cathodes. After 500 cycles, the discharge specific capacity of Al-doped cathode materials was around 150 mAh g⁻¹ reflecting 81% capacity retention. For the cells with cathodes containing the Ti-doped material, the discharge capacity after 500 cycles was around 124 mAh g⁻¹, reflecting an average capacity retention around 65%. In turn,

cells with reference cathodes showed after 500 cycles a specific capacity around 100 mAh g⁻¹, reflecting a capacity retention around 52%.

The thermal behavior of the NCM85 reference, Al-doped and Ti-doped materials in the presence of the electrolyte solution (EC-EMC/LiPF₆) was studied by differential scanning calorimetry, as shown in Figure 9. The first minor peaks in the range of ~72–79 °C appearing for both reference and doped materials are related to the exothermic reactions between the electrolyte solution species and the surface Li₂CO₃ species (Figure 9, Zone I) which is in line with our previous studies.^[20] The onset temperatures, corroborate to the major exothermic reactions were found to be close: 214 °C, 216 °C and 218 °C for NCM85 reference, Ti- and Al-doped materials, respectively. The specific total heat release was found to be $Q_{\text{total}} = 468 \pm 5$, 376 ± 2 , and 352 ± 2 J g⁻¹ for the reference, Al- and Ti-doped NCM85 materials, respectively which shows ~24–33% lower heat evolutions for the doped samples (Figure 9, Zone II). The exothermic heat evolution is typically related to (i) the reactions between the released lattice oxygen with the solvents and (ii) the combustion reaction of solvents with the NCM materials.^[26,27] Hence, the results of these thermal studies correlate well with the positive effect of doping NCM85 with Al and Ti on the structural and electrochemical stability of these cathode materials. It can be generalized that improving the electrochemical stability of many electrodes materials for batteries (via bulk or surface treatments) is coherent with their thermal stabilization as well.

It is important to note that a full understanding of why and how doping Ni-rich NCM cathode materials by very small amounts of multivalent metallic cations stabilizes the electrochemical and morphological response of these cathodes during cycling is not fully understood and deserve more experimental and theoretical work. It is also hard to understand at this stage the difference in the effect of Al and Ti as we found in this work. One obvious possibility is a different level of distribution of the dopants in the Ni–Co–Mn oxide matrices due to difference in solubility and diffusion during the synthetic route. Taking into account the low concentration of the dopants involved, much more work (both experimental and theoretical)

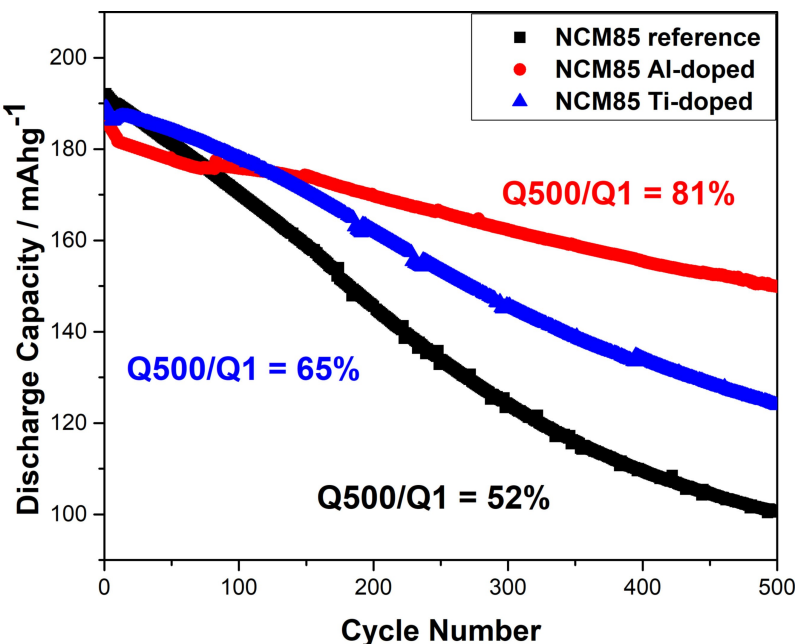


Figure 8. Extended cycling performance of NCM85 reference, Al-doped and Ti-doped cathodes tested in pouch-type full cells with graphite anodes at discharge rate of 1 C, 1 M LiPF₆ in EC-EMC 3:7 by volume, 30 °C.

is required, in order to decipher the right explanation (much beyond the scope of this work).

However, an extensive computational work that was carried out on doped NCM cathode materials can provide some clues regarding their mechanisms of influence. Consequently, several interesting studies are briefly discussed below. These authors have reported on several studies that use first-principles density functional theory (DFT) calculations to elucidate the role of the oxidation states of Ni ions on the stability of NCM523 and NCM622 materials.^[8–9,16] These studies showed that the availability of red-ox active electrons and ionic Ni–O interactions renders Ni²⁺ oxidation state preferable to Ni³⁺ and Ni⁴⁺ oxidation state. Doping with high-valent metal ions improves the stability by charge compensation and eventually increases the stability of cathode material during repeated Li insertion/de-insertion along a potential range between 3.0 and 4.3 V vs. Li. Min et al. showed that doping LiNi_{0.8}Co_{0.1}Mn_{0.1}O₂ with Al stabilizes the fully lithiated NCM material by preventing formation of oxygen vacancies which are strongly connected to cation disordering. Thereby, Al doping can effectively prevent Ni ions migration into Li sites, even at the de-lithiated state, in which oxygen vacancies may be formed.^[12]

Kim et al. explored the effect of doping by Zr on LiNiO₂ (LNO) doping with Zr, using DFT calculations.^[17] They could determine that in the bulk crystal, the dopant preferentially substitutes Ni, but during charging, as the cathode material becomes Li-deficient, the dopant migrated to Li sites, in what is called the “pillar effect”. They also suggested that the dopant cations tend to segregate around the surface region. This segregation results in suppression of detrimental oxygen release from the cathode surface region, by forming favorable interactions of the dopant cations with oxygen atoms at the

surface. These interactions stabilize reactive surface oxygen moieties, thus reducing their parasitic reactions with the alkyl carbonate solvents molecules.

Another important study on the effect of seven dopants: Al, Ti, Ga, Mg, Si, V and Zr on the stability of LiNi_{1-2x}Co_xMn_xO₂ ($x \leq 1/12$) was performed by Liang et al. using first principles based calculations.^[18] They concluded that cation doping usually happens at Co and Mn sites, while the Ni sites remain initially unchanged. Moreover, doping at different doping sites has diverse influences – doping at Mn sites reduces Li/Ni cation mixing and oxygen evolution, while doping at Co sites improves the phase stability, uniformity and charge-transfer. Among the various dopants examined, Al was found to be the best candidate for Mn sites doping, and Ti or Zr have proved to be the best candidates for Co sites doping. The authors concluded that each dopant has its own advantages and drawbacks, so there is no single “magic” dopant that overcomes all different drawbacks of Ni-rich NCM cathode materials.

As this brief review of the theoretical studies suggests, several specific aspects of doping are understood, but a general theory that provides clear guidelines was not elaborated yet. It is also apparent that several different factors play a role in determining the efficiency of doping. Moreover, as Liang et al. suggested, it is likely that each metal ion utilizes a somewhat different doping mechanism, resulting in different effects on the cathode materials, some are favorable and some are not. Finally, each cathode composition has its own chemical uniqueness and requires its own specialized study.

The knowledge accumulated so far by the computational work (part of which is described briefly above) seems to suggest that doping NCM85 by either Al or Ti cations reduces

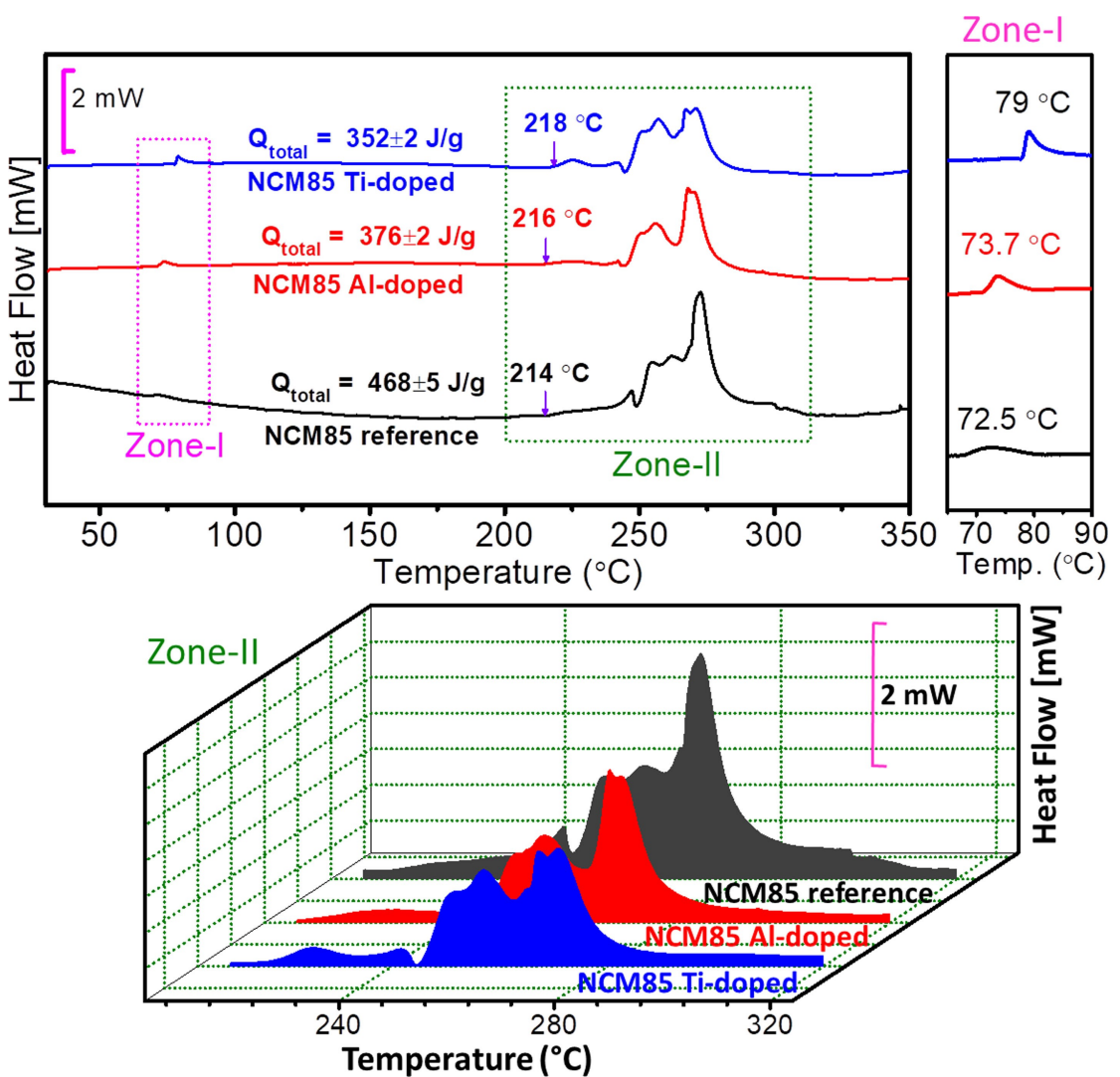


Figure 9. DSC measurements of NCM85 reference, Al-doped and Ti-doped cathode materials in contact with the electrolyte solution used in this work. The temperature scanning rate was 1 °C/min.

oxygen evolution by segregating near the particles' surface area, forming strong bonds with O and constructing a protective layer that prevents the formation of cracks near the active mass surface. In addition, it is likely that their incorporation in the bulk material makes the more stable Ni²⁺ oxidation state preferable over Ni³⁺ and Ni⁴⁺ oxidation states, and therefore stabilizes the bulk structure. It is also possible that Al and Ti dopants in these materials promote formation of what Kim et al. described as the "pillar effect", thus during cycling they migrate to Li sites. The question of why NCM85 Al-doped material has better electrochemical and structural properties than NCM85 Ti-doped is still open, and further investigation is required. The difference between Al and Ti doping effects on the electrochemical and structural characteristics may provide some clues about the underlying doping mechanisms. One favorite explanation (yet at the speculative level) is the metal ions' site occupation differences, pointed out by Liang and el. To better understand this mechanism and to derive more conclusive explanations, we are collecting and

analyzing additional data on a variety of dopants for NCM85 cathode materials in a follow-up, on-going work.

3. Conclusions

In this work, we examined the influence of Al and Ti doping on the structural, electrochemical and thermal properties of NCM85 cathode materials. By using multiple characterization tools such as XRD, HR-SEM, TEM, and EDX, we analyzed the phases existing, crystal structure and morphology of the different samples, and concluded that upon doping with 0.3 mol% of Al and Ti these materials do not undergo observable changes in these aspects. However, electrochemical testing of these cathodes showed the superiority of the Al-doped cathode material over the Ti-doped and undoped materials in half (vs. Li) and full (vs. graphite) cells measured at 2 temperatures and different rates. Examination of the electrochemical results implies that doping with Al and Ti facilitates

the Li intercalation and de-intercalation processes. FIB-SEM images of the cycled cathodes showed that the doping with Al, and to a minor degree with Ti, reduces the formation of cracks in the particles upon cycling, what is considered as a major capacity fading mechanism of these cathodes. The results presented herein demonstrate the coherence among structural, electrochemical and thermal stabilization that was achieved by doping. At this stage we hesitate to suggest a clear mechanism that explains the positive effect of doping by foreign multi-valent metal cations at such small amounts. We may be fully conclusive after completing follow-up studies with other dopants and extensive computational work.

Experimental Section

Synthesis of cathode materials

The NCM85 reference, Al 0.3 mol % doped, and Ti 0.3 mol % doped cathode materials were synthesized using conventional solid-state method. $\text{Ni}_{0.85}\text{Co}_{0.1}\text{Mn}_{0.05}(\text{OH})_2$ and LiOH precursors supplied by BASF SE were mixed together with suitable amounts of doping agents, namely, Al_2O_3 or TiO_2 , for the doped materials. The mixed powders were calcinated at 760 °C for 6 hours under constant O_2 gas flow. We conducted preliminary cycling tests of electrodes comprising doped NCM materials. We examined 1% and 0.3% mole doped materials and found the latter ones being slightly better. It did not make sense to use dopants concentrations below 0.3%. Since the difference between 0.3% and 1% doping was small, it was easy to conduct the work using 0.3% mole of dopants.

Characterizations of cathode materials

Chemical analysis of the synthesized materials was carried out using the inductive coupled plasma technique (SPECTRO ARCOS ICP-OES Multi view FHX22). The crystalline phase of the uncycled and cycled cathodic materials was examined using powder X-ray diffraction (XRD) by a Bruker D8 ADVANCED diffractometer with Cu radiation ($\lambda\text{CuK}\alpha = 1.54 \text{ \AA}$). The data was measured in a 2θ range from 10° to 80°, with a scan rate of 5θ per minute. High-resolution scanning electron microscope (HR-SEM, FEI, Magellan 400 L) was used to analyze the particle size, morphology and surface composition of the cathodic material. TEM investigations were performed using an analytical high-resolution transmission electron microscope JEOL-2100 with a LaB₆ gun operating at 200 kV. Thin specimens for TEM were prepared with a focused ion beam (FIB) tool (Helios 600, FEI).

Electrochemical tests

The electrochemical properties were characterized using 2325 coin-type cells with Li foil counter electrodes and (full) pouch cells with graphite counter electrodes. Positive electrodes were prepared by coating Al foils current collectors with homogenous mixed slurries of active material, P65 carbon black, KS6 graphite and Solef 5130 polyvinylidene fluoride (PVDF) binder with a weight ratio of 94:1:2:3 in N-pyrrolidone (NMP) solvent. The wet electrodes were dried at 120 °C overnight in vacuum. The positive electrodes have an average active mass density of 10 mg cm⁻³. The average loading of the cathodes in the coin cells was 1.85 mAh/cm². The coin-cells were assembled in an Argon-filled glove box and composed of a positive electrode, Li metal as negative electrode, Celgard PP2500 separators and electrolyte composed of 1.0 M LiPF₆ dissolved

ethylene in carbonate and ethyl methyl carbonate, 3:7 v:v mixture (LP57, BASF SE). For the full pouch cells we used the same components, except for the negative electrodes which were based on graphite with a capacity excess of 10% over that of the cathodes. The graphite electrodes comprised 92% graphite ("Formula BT" of Superior Graphite comp.), 3% carbon black and 5% PVDF in NMP.

Initial charge-discharge capacities, rate capability, and cycling performance were measured by a MACCOR multichannel computerized battery testing system in a voltage range of 3.0–4.3 V at 30 °C and 45 °C, in thermostats. Impedance measurements were measured by frequency response analyzer (FRA-1255) from Solartron, Inc.

Thermal measurements

The differential scanning calorimetry (DSC) analyses were performed in the range between room temperature and 350 °C (DSC 3 + STARe System, METTLER TOLEDO) using closed reusable high pressure gold-plated stainless steel crucibles (30 μL in volume). All the weighing measurements were done using a microbalance (Mettler Toledo AB135-S/FACT).

Conflict of Interest

The authors declare no conflict of interest.

Keywords: Ni-rich cathode materials • Li-ion batteries • Al doping • Ti doping • $\text{LiNi}_{0.85}\text{Co}_{0.1}\text{Mn}_{0.05}\text{O}_2$

- [1] C. M. Hayner, X. Zhao, H. H. Kung, *Annu. Rev. Chem. Biomol. Eng.* **2012**, 3, 445.
- [2] N. Nitta, F. Wu, J. T. Lee, G. Yushin, *Mater. Today* **2015**, 18, 252.
- [3] A. Manthiram, B. Song, W. Li, *Energy Storage Mater.* **2017**, 6, 125.
- [4] H.-J. Noh, S. Youn, C. S. Yoon, Y.-K. Sun, *J. Power Sources* **2013**, 233, 121.
- [5] W. Liu, X. Li, D. Xiong, Y. Hao, J. Li, H. Kou, B. Yan, D. Li, S. Lu, A. Koo, *Nano Energy* **2018**, 44, 111.
- [6] C. Chen, T. Tao, W. Qi, H. Zeng, Y. Wu, B. Liang, Y. Yao, S. Lu, Y. Chen, *J. Alloys Compd.* **2017**, 709, 708.
- [7] T. Weigel, F. Schipper, E. M. Erickson, F. A. Susai, B. Markovsky, D. Aurbach, *ACS Energy Lett.* **2019**, 4, 508–516.
- [8] D. Aurbach, O. Srur-Lavi, C. Ghanty, M. Dixit, O. Haik, M. Taliander, Y. Grinblat, N. Leifer, R. Lavi, D. T. Major, *J. Electrochem. Soc.* **2015**, 162, A1014.
- [9] M. Dixit, B. Markovsky, D. Aurbach, D. T. Major, *J. Electrochem. Soc.* **2017**, 164, A6359.
- [10] U.-H. Kim, S.-T. Myung, C. S. Yoon, Y.-K. Sun, *ACS Energy Lett.* **2017**, 2, 1848.
- [11] Y.-C. Li, W. Xiang, Z.-G. Wu, C.-L. Xu, Y.-D. Xu, Y. Xiao, Z.-G. Yang, C.-J. Wu, G.-P. Lv, X.-D. Guo, *Electrochim. Acta* **2018**, 291, 84.
- [12] K. Min, S.-W. Seo, Y. Y. Song, H. S. Lee, E. Cho, *Phys. Chem. Chem. Phys.* **2017**, 19, 1762.
- [13] W. Cho, J. H. Song, K.-W. Lee, M.-W. Lee, H. Kim, J.-S. Yu, Y.-J. Kim, K. J. Kim, *J. Phys. Chem. Solids* **2018**, 123, 271.
- [14] Y. Zhang, Z.-B. Wang, J. Lei, F.-F. Li, J. Wu, X.-G. Zhang, F.-D. Yu, K. Ke, *Ceram. Int.* **2015**, 41, 9069.
- [15] F. A. Susai, D. Kovacheva, A. Chakraborty, T. Kravchuk, R. Ravikumar, M. Taliander, J. Grinblat, L. Burstein, Y. Kauffmann, D. T. Major, *ACS Appl. Mater. Interfaces* **2019**, 2, 4521–4534.
- [16] F. Schipper, M. Dixit, D. Kovacheva, M. Taliander, O. Haik, J. Grinblat, E. M. Erickson, C. Ghanty, D. T. Major, B. Markovsky, *J. Mater. Chem. A* **2016**, 4, 16073–16084.
- [17] Y. Kim, *Phys. Chem. Chem. Phys.* **2019**, 21, 12505–12517.
- [18] C. Liang, F. Kong, R. C. Longo, C. Zhang, Y. Nie, Y. Zheng, K. Cho, *J. Mater. Chem. A* **2017**, 5, 25303–25313.

- [19] A. Purwanto, C. S. Yudha, U. Ubaidillah, H. Widiyandari, T. Ogi, H. Haerudin, *Mater. Res. Express* **2018**, *5*, 122001.
- [20] J. Xu, F. Lin, M. M. Doeff, W. Tong, *J. Mater. Chem. A* **2017**, *5*, 874–901.
- [21] A. Chakraborty, S. Kunnikuruvan, S. Kumar, B. Markovsky, D. Aurbach, M. Dixit, D. T. Major, *Chem. Mater.* **2020**, *32*, 915–952.
- [22] C. S. Yoon, M. H. Choi, B.-B. Lim, E.-J. Lee, Y.-K. Sun, *J. Electrochem. Soc.* **2015**, *162*, A2483.
- [23] H.-H. Sun, A. Manthiram, *Chem. Mater.* **2017**, *29*, 8486.
- [24] Z. Xu, M. M. Rahman, L. Mu, Y. Liu, F. Lin, *J. Mater. Chem. A* **2018**, *6*, 21859.
- [25] Q.-C. Zhuang, X.-Y. Qiu, S.-D. Xu, Y.-H. Qiang, S.-G. Sun, *Lithium Ion Batteries—New Developments* **2012**, *8*, 189–227.
- [26] O. Haik, F. S. Amalraj, D. Hirshberg, L. Burlaka, M. Talianker, B. Markovsky, E. Zinigrad, D. Aurbach, J. K. Lampert, J.-Y. Shin, *J. Solid State Electrochem.* **2014**, *18*, 2333–2342.
- [27] T. Inoue, K. Mukai, *ACS Appl. Mater. Interfaces* **2017**, *9*, 1507–1515.

Manuscript received: August 14, 2020
Accepted manuscript online: September 12, 2020
Version of record online: October 15, 2020